

Feedback-Enhanced Driven-Dissipative Quantum Batteries in Waveguide-QED Systems

Xian-Li Yin,¹ Meixi Guo,¹ Jian Huang,² Heung-wing Joseph Lee,¹ and Guofeng Zhang^{1,3,4}

¹*Department of Applied Mathematics, The Hong Kong Polytechnic University, Kowloon 999077, Hong Kong, China*

²*Department of Physics, City University of Hong Kong, Kowloon, Hong Kong SAR*

³*The Hong Kong Polytechnic University Shenzhen Research Institute, Shenzhen, Guang Dong 518057, China*

⁴*Research Institute for Quantum Technology, The Hong Kong Polytechnic University, Hong Kong, China*

(Dated: November 11, 2025)

Quantum batteries (QBs), acting as energy storage devices, have potential applications in future quantum science and technology. However, the QBs inevitably losses energy due to their interaction with environment. How to enhance the performance of the QBs in the open-system case remains an important challenge. Here we propose a scheme to realize the driven-dissipative QBs in atom-waveguide-QED systems and demonstrate significant improvements in both the stored energy and extractable work (ergotropy) of the QBs via feedback control. For a single-atom QB, we show that combining the measurement and coherent feedback controls enables nearly perfect stable charging under the weak coherent driving. For the QB array, the measurement-based feedback allows us to control different dynamical phases in the thermodynamic limit: (i) a continuous boundary time-crystal phase, where persistent periodic energy charge-discharge oscillations emerge despite the presence of the dissipation into the waveguide, and (ii) two stationary phases—one reaches full charge while the other maintains only small energy storage. This work broadens the scope of driven-dissipative QBs and provides practical strategies for enhancing their performance.

I. INTRODUCTION

The rapid development of quantum technologies has created an urgent demand for efficient quantum energy storage devices [1–3]. Quantum batteries (QBs), first proposed by Alicki and Fannes [4], utilize quantum mechanical principles to achieve superior performance in charging power and work extraction compared to classical counterparts [5–14]. Early theoretical studies in closed systems have revealed remarkable advantages through unitary charging protocols and collective quantum effects [15–26]. However, the practical implementation of QBs remains hindered by the decoherence-induced energy loss and dissipative charging dynamics in open quantum environments. To address these challenges, various approaches have been proposed [27–47], such as utilization of non-Markovian effects [36–40], Floquet engineering [41], dark state [42], and feedback control [43–45]. Experimental realizations of QBs have also been demonstrated across diverse platforms, including superconducting circuits [48, 49], quantum dots [50], organic microcavities [51], and nuclear spins [52].

Waveguide quantum electrodynamics (QED) systems [53–56] have emerged as a promising platform for studying and realizing QBs. Existing implementations typically rely on passive energy transfer mechanisms, such as remote wireless charging mediated by atom-photon bound states [39, 40] or collective effect against the energy loss of the QBs [57]. These passive mechanism, however, fundamentally differs from the driven-dissipative regime [27–35], where the external laser field continuously pumps the charger or QBs while the dissipation caused by the fields in the waveguide maintains. The competition between the driving and dissipation may create rich non-equilibrium dynamics [58–60] that render conventional protocols ineffective. To address this, feedback control [61–66] offers a pathway to not only mitigate the decoherence effects but also to actively exploit the driven-dissipative environment for enhancing the performance of QBs. The key open question we address is how to implement such control to boost the stored energy under continuous driving.

In this work, we propose a driven-dissipative two-level-atom QB scheme via coupling the atoms to a one-dimensional waveguide. Taking advantage of feedback control, the performance of both the single-atom QB and multiple-atom QB array can be significantly improved. For the charging process in the single-atom QB, it can be injected more stable energy when the measurement feedback (MFB) control [61, 62, 66] is applied to the system. Furthermore, by incorporating the coherent feedback (CFB) control [63–65], the performance of the QB is further improved even in the achiral-coupling case. In the collective charging process of the multiple-atom QB array, the synergistic effect between the MFB control and external driving gives rise to different dynamical phases in the thermodynamical limit. We find that the QB array can exhibit persisting oscillation in the continuous boundary time-crystal (BTC) phase [58] and store more stable energy in one of the stationary phases. Our results provide new insights into the design of QBs in open quantum systems.

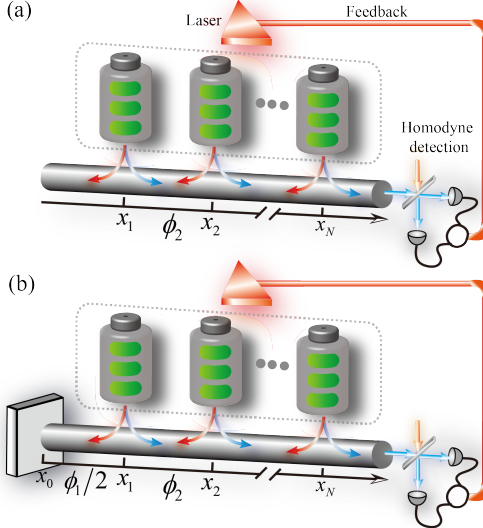


FIG. 1. Schematic of two different setups of the quantum battery (QB). (a) Setup I, a QB array (modeled as two-level atoms) is coupled to an open waveguide. (b) Setup II, a QB array is coupled to a semi-infinite waveguide, whose end lying at $x_0 = 0$ behaves as a perfect mirror. In both setups, an external laser persistently input energy into the QB array. The right-emitted photons are monitored via a homodyne detection, producing a corresponding photocurrent that is fed back to modulate the external laser field.

II. DRIVEN-DISSIPATIVE-CHARGING QB MODEL

We consider that a QB array, modeled as an ensemble of two-level atoms with resonance frequency ω_0 , is coupled to either an open or a semi-infinite waveguide, as shown by setups I and II in Figs. 1(a) and 1(b), respectively. The single-atom spontaneous decay rates into the right- and left-propagating modes are γ_R and γ_L , respectively, with a total decay rate $\gamma = \gamma_R + \gamma_L$. An external laser with driving amplitude Ω persistently input energy into the QB array to compete with the system dissipation. Photons emitted into the right-propagating mode are monitored via continuous homodyne detection of the phase quadrature $P(t)$ of the photocurrent. The measured photocurrent is then fed back into the system, which can instantaneously modify the driving amplitude of the laser. Within the Born-Markov approximation framework and using the SLH formalism [67–70], the quantum master equations describing the driven-dissipative dynamics of setups I and II are, respectively, given by [71]

$$\dot{\rho}_I = -i[H_{RL} + H_{f,I} + H_d, \rho_I] + D[L_R - iF]\rho_I + D[L_L]\rho_I, \quad (1a)$$

$$\dot{\rho}_{II} = -i[H_{RL} + H_{f,II} + H_{\phi_1} + H_d, \rho_{II}] + D[e^{i\phi_1} S_R L_L + L_R - iF]\rho_{II}. \quad (1b)$$

The exchanging interaction mediated by the waveguide is given by $H_{RL} = \frac{\gamma_R}{2i} \sum_{j>l} e^{i\phi_{l,j}} \sigma_j^+ \sigma_l^- + \frac{\gamma_L}{2i} \sum_{j< l} e^{i\phi_{l,j}} \sigma_j^+ \sigma_l^- + \text{H.c.}$, where $\phi_{l,j} = k_0|x_j - x_l|$ being the propagating phase of photons between the positions x_l and x_j , $k_0 = \omega_0/v_g$ is the wave vector of the field at frequency ω_0 , and v_g is the corresponding group velocity; $H_{f,I} = F^\dagger L_R/2 + \text{H.c.}$ and $H_{f,II} = F^\dagger (e^{i\phi_1} S_R L_L + L_R)/2 + \text{H.c.}$ are the Hamiltonians induced by the MFB control in the case of setups I and II, respectively, where $F = i\sqrt{\gamma_R g} \sum_i \sigma_i^x$ denotes the feedback operator, with g being the feedback strength; $D[o] \bullet = o \bullet o^\dagger - \{o^\dagger o, \bullet\}/2$ is the Lindblad superoperator, where the right and left collapse operators are, respectively, given by $L_R = \sqrt{\gamma_R} \sum_{j=1} e^{i\phi_{\Sigma_R}} \sigma_j^-$ and $L_L = \sqrt{\gamma_L} \sum_{j=1} e^{i\phi_{\Sigma_L}} \sigma_j^-$, with $\phi_{\Sigma_R} = \sum_{s=j+1}^N \phi_s$, and $\phi_{\Sigma_L} = \sum_{s=2}^j \phi_s$; $H_{\phi_1} = e^{i\phi_1} S_R L_R^\dagger L_L/2i + \text{H.c.}$ is the Hamiltonian induced by the CFB control; $H_d = \Omega \sum_{j=1}^N \sigma_j^x$ is the driving Hamiltonian; $S_R = S_L = e^{i\phi_\Sigma}$ are the scattering matrices for the right- and left-propagating modes, with $\phi_\Sigma = \sum_{s=2}^N \phi_s$.

To characterize the performance of the driven-dissipative QB in setups I and II, we introduce the stored energy at time t , defined as $\mathcal{E}(t) = \text{Tr}[H_B \rho_B(t)]$. Here, H_B and $\rho(t)$ are, respectively, the bare energy and density matrix of the atoms. This characterization is justified under the typical condition where $\omega_0 \gg \gamma, \Omega$ [72–74]. The second law of thermodynamics shows that not all of $\mathcal{E}(t)$ is available for work extraction. The maximum work that can be extracted from the state $\rho(t)$ of the QB is called ergotropy, defined as $\mathcal{W}(t) = \text{Tr}[\rho(t)H_B] - \text{Tr}[\sigma(t)H_B]$ [75, 76], where $\sigma(t) = \sum_n r_n(t)|\epsilon_n\rangle\langle\epsilon_n|$ is the passive state. Here, $r_n(t)$ are the eigenvalues of $\rho(t)$ sorted in decreasing order, $r_1 \geq r_2 \geq \dots \geq r_N$, and $|\epsilon_n\rangle$ are the eigenstates of H_B with the corresponding eigenvalues ϵ_n sorted in an increasing

order, $\epsilon_1 \leq \epsilon_2 \leq \dots \leq \epsilon_N$.

III. FEEDBACK-ENHANCED SINGLE-ATOM QB

In order to elucidate the charging mechanism in the presence of feedback control, we first focus on the single-atom driven-dissipative QB. According to Eq. (1a), the dynamics of the QB in setup I is given by the Lindblad master equation

$$\dot{\rho}_I = i[\rho_I, \Omega\sigma^x] + \sum_{\mu, \nu=+, -} \Gamma_{\mu\nu}^{(I)} D_{\sigma^\mu, \sigma^\nu} \rho_I, \quad (2)$$

where the feedback-strength-dependent decay rates are given by $\Gamma_{-+}^{(I)} = \gamma_R(g+1)^2 + \gamma_L$, $\Gamma_{+-}^{(I)} = \gamma_R g^2$, and $\Gamma_{++}^{(I)} = \Gamma_{--}^{(I)} = \gamma_R g(g+1)$, and $D_{\sigma^\mu, \sigma^\nu} \bullet = \sigma^\mu \bullet \sigma^\nu - \{\sigma^\nu \sigma^\mu, \bullet\}/2$. It is interesting to see that the master equation (2) has the same form as that of a driving two-level atom in a squeezed vacuum reservoir [77–80]. By adjusting the feedback strength g , we can enhance or suppress the decay process of the QB and hence achieve different stable charging.

From the decay rates in Eq. (2), one can find that the components γ_L in $\Gamma_{-+}^{(I)}$ is independent of g . In our scheme, only the right-propagating photons are measured by the homodyne detector. As a result, the jump operator associated with left-propagating modes remains unchanged. To address this issue, we further investigate the charging performance in setup II, where the waveguide end behaves as a perfect mirror. The photons emitted to the left-propagating modes will be reflected back to the atoms, and hence the dynamics of the atoms can also be controlled by the CFB control [63–65]. The master equation for the single-atom QB in setup II is obtained as

$$\dot{\rho}_{II} = i[\rho_{II}, \Omega\sigma^x + \omega\sigma^+\sigma^-] + \sum_{\mu, \nu=+, -} \Gamma_{\mu\nu}^{(II)} D_{\sigma^\mu, \sigma^\nu} \rho_{II}, \quad (3)$$

with the frequency shift $\omega = \sqrt{\gamma_R\gamma_L} \sin \phi_1(g+1)$ and decay rates $\Gamma_{-+}^{(II)} = \gamma + \gamma_R g(g+2) + 2\sqrt{\gamma_R\gamma_L}(g+1) \cos \phi_1$, $\Gamma_{+-}^{(II)} = \gamma_R g^2$, and $\Gamma_{++}^{(II)} = (\Gamma_{--}^{(II)})^* = \gamma_R g(g+1) + \sqrt{\gamma_R\gamma_L} g e^{-i\phi_1}$. Owing to the CFB control, the decay rate associated with the left-propagating mode can also be adjusted by the feedback strength. The CFB control is engineered by the propagating phase ϕ_1 , which can enhance or suppress the decay of the QB dynamics. In the absence of the MFB control, if the phase is fixed at $\phi_1 = \pi$, the two-level atom is completely decoupled from the waveguide [63–65], and hence the energy stored in the QB can exhibit a periodical oscillation, with a period determined by the driving frequency of the laser. In the driven-dissipative regime, we fix $\phi_1 = 2\pi$ and consider the achiral (bidirectional) coupling case ($\gamma_R = \gamma_L = \gamma/2$). Under these conditions, we can investigate the combined effects of the driving, dissipation, and feedback controls, while the chiral-coupling case is discussed in the Supplementary Information [71].

From the dynamics of the density matrix elements, the QB in the long-time limit evolves into the steady state

$$\rho_i^{ss} = \frac{1}{\eta_i} \begin{pmatrix} \varsigma_i & -4i(g+1)\gamma\Omega \\ 4i(g+1)\gamma\Omega & \eta_i - \varsigma_i \end{pmatrix}, \quad (4)$$

where $i = \text{I}$ and II are used to label the two different QB setups. The two eigenvalues of ρ_i^{ss} are given by $r_\pm = 1/2 \pm \chi_i/\eta_i$. The specific forms of the parameters η_i , ς_i , and χ_i are presented in the SM [71], which strongly depend on the driving amplitude Ω and the MFB control strength g .

The steady-state energy-storage performance of the QB in setups I and II is evaluated as a function of the driving amplitude Ω and MFB control strength g in Figs. 2(a) and 2(b), where we see that the feedback strength g approximately partitions the energy landscape into three distinct regions, labeled A, B, and C, respectively. The steady-state energies in regions B and C are significantly influenced by both Ω and g , with region C supporting the highest steady-state energy. In contrast, the energy in region A is largely insensitive to these parameters. The comparison of \mathcal{E}_I^{ss} and \mathcal{E}_{II}^{ss} further indicates that the QB in setup II exhibits superior energy-storage performance in the driven-dissipative regime, which achieves a larger steady-state energy in a fairly wide parameter regime. Furthermore, under the weak driving case $\Omega/\gamma \ll 1$, the QB in setup II can approach the full-charge limit.

Figs. 2(c) and 2(d) compare the time evolutions of the energy and ergotropy for these two setups. When $g = -2$, the MFB control significantly boosts the charging process and enhances the maximal ergotropy in both cases. For setup II, the evolution of $\mathcal{W}_{II}(t)$ closely follows that of $\mathcal{E}_{II}(t)$, indicating high extractable work of the QB. For setup I, however, the steady-state ergotropy is much smaller than the stored energy due to losses into the left-propagating waveguide mode. A critical finding is that at $g = -1$, the steady-state density matrix becomes fully mixed, with vanishing coherence (off-diagonal elements). Consequently, the steady-state energy saturates at 1/2, and no work can be extracted from the QB. These results show that by appropriately tuning the feedback strength g and driving amplitude Ω , the charging performance of a single-atom QB can be effectively enhanced.

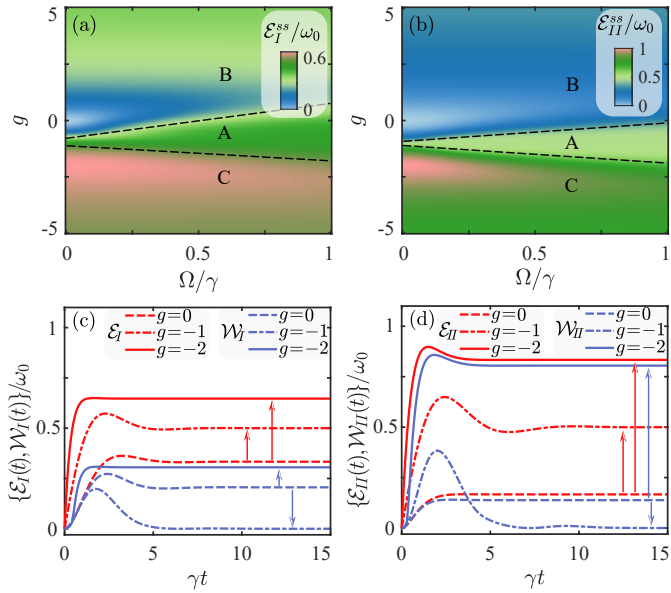


FIG. 2. Steady-state energy \mathcal{E}_I^{ss} (a) and \mathcal{E}_{II}^{ss} (b) versus the driving amplitude Ω and feedback strength g . Time evolutions of the energy and ergotropy for setups I (c) and II (d), comparing the cases with $g = 0$ (without MFB) and $g = -1, -2$ (with MFB). In panels (c) and (d), the driving amplitude is fixed at $\Omega/\gamma = 0.5$. Other parameters used are $\Delta\gamma = 0$ and $\phi_1 = 2\pi$.

IV. MANY-BODY PHASE-CONTROLLED QB ARRAY

After establishing the role of the feedback control in enhancing the single-atom QB, we now extend our analysis to the many-body charging behavior of N two-level atoms serving as a QB array. In this case, the MFB control can be used to engineer rich dynamical phases due to the multiple-atom collective effect [66, 81]. By positioning the atoms to satisfy $\phi_i = 2m\pi$ ($i = 1, 2, \dots, N$ and $m \in \mathbb{Z}$), the quantum master equations in Eqs. (1a) and (1b) are reduced to the unified form

$$\dot{\rho} = i \left[\rho, 2\Omega J_x - \frac{n\gamma g}{2} \{ J_x, J_y \} \right] + \sum_{\mu, \nu = +, -} \Gamma_{\mu\nu} D_{J_\mu, J_\nu} \rho, \quad (5)$$

where $J_{\alpha=x,y,z} = \sum_{j=1}^N \sigma_j^\alpha / 2$ and $J_\pm = J_x \pm i J_y$ are the collective operators. The index $n = 1$ and 2 correspond to setups I and II, respectively, with the decay rates $\Gamma_{-+} = \gamma[g^2 + 2n(g+1)]/2$, $\Gamma_{+-} = g^2/2$, and $\Gamma_{++} = \Gamma_{--} = g(g+n)/2$. Therefore, the constructive interference of propagating photons in the waveguide yields a collective spin mode of length $N/2$ [82–84].

In the QB array, the stored energy is defined as $\mathcal{E}/N\omega_0 = (\langle J_z \rangle/N) + 1/2$, with the expectation value defined as $\langle \bullet \rangle = \text{Tr}[\bullet \rho]$. We consider the thermodynamics limit $N \rightarrow \infty$ and introduce the expectation values for the magnetization vector components $m_\alpha = \langle J_\alpha \rangle/N$ [58]. When $N \rightarrow \infty$, the dynamics of the expectation values is exactly governed by the mean-field equations [71]: $\dot{m}_x = n\Gamma m_z m_x$, $\dot{m}_y = -2\Omega m_z + n\Gamma \xi m_y m_z$, and $\dot{m}_z = 2\Omega m_y - n\Gamma m_x^2 - n\Gamma \xi m_y^2$, with $\xi = 2g + 1$. To ensure a well-defined thermodynamic limit, we introduce the rescaled decay rate $\Gamma = N\gamma$ for the $N/2$ spin. The mean-field equations conserve the length j of the average magnetization vector $\vec{m} = [m_x(t), m_y(t), m_z(t)]$. In addition, the system exists another conserved quantity $\mathcal{M} = \Gamma m_x^2 / (\Gamma m_y - \Omega)$ [71], which thus constrains the magnetization dynamics to a specific trajectory. For the many-body charging process, we consider that the N atoms are initially in their ground state, with the initial condition $m_x(0) = m_y(0) = 0$ and $m_z(0) = -1/2$. Therefore, we have $j = 1/4$ and $\mathcal{M} = 0$. It is found that there exists two stationary phases and a BTC phase in both setups I and II. When the driving amplitude satisfies $\Omega > \Omega_{\text{cri}} = n\Gamma|\xi|/4$, the energy stored in the QB array will exhibit persistent oscillations even when the atoms decay to the fields in the waveguide. In contrast, the time evolution of the stored energy in the QB array approaches two stationary values $\mathcal{E}^{ss} = -\text{sign}(\xi) \sqrt{1/4 - 4\Omega^2/n^2\Gamma^2\xi^2} + 1/2$ [71], whose sign depends on the feedback strength. For $\xi \geq 0$ (i.e., $g \geq -1/2$), we find that $\mathcal{E}^{ss} \leq 1/2$ holds for both setups I and II. This behavior is consistent with the steady-state charging energy achieved via collective effect in the driven-dissipative regime without feedback control [30]. While for $\xi < 0$ (i.e., $g < -1/2$), the relation $\mathcal{E}^{ss} > 1/2$ holds for both setups. The stability of these two stationary solutions can be checked by examining the eigenvalues of the Jacobian matrix J [85]. We see that the critical driving amplitude Ω_{cri} and the steady-state stored energy \mathcal{E}^{ss} in setups I and II

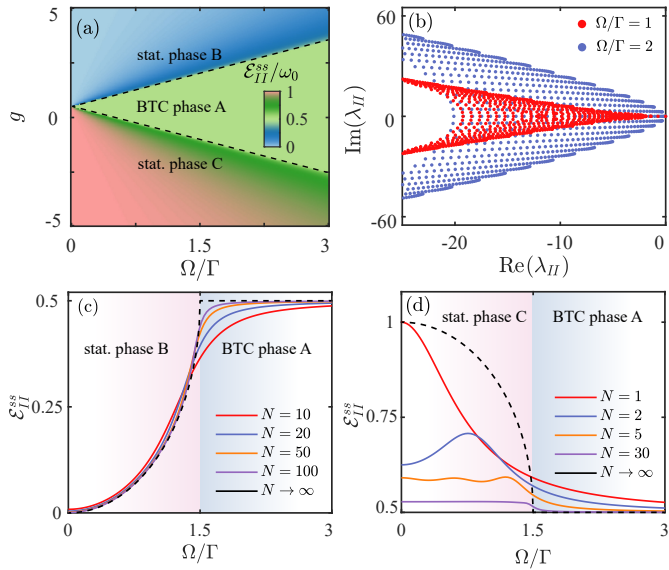


FIG. 3. (a) Steady-state energy \mathcal{E}_{II}^{ss} versus Ω and g . (b) Eigenvalues λ_{II} of the Liouvillian \mathcal{L} are shown in the boundary time-crystal phase A ($\Omega/\Gamma = 2$, blue dots) and in the stationary phase B ($\Omega/\Gamma = 1$, red dots) with $g = 1$. (c) and (d) Steady-state energy \mathcal{E}_{II}^{ss} as a function of Ω at $g = 1$ and $g = -2$, respectively. Dashed lines are the mean-field results for $N \rightarrow \infty$ and solid lines are obtained by finding the steady state of Eq. (5) for setup II with various atom numbers N .

have the similar form in the thermodynamic limit. Therefore, we focus on the charging behavior of the QB array in setup II. A comparison of the charging performance for these two setups in finite system size is presented in the Supplementary Information [71].

Figure 3(a) illustrates that the steady-state energy \mathcal{E}_{II}^{ss} is well divided into three distinct dynamical regions by the critical driving amplitude Ω_{cri} (as shown by the black dashed lines): BTC phase A, and stationary phases B and C. As we will show, the QB array exhibits persistent oscillatory dynamics in the phase A, while it relaxes to two distinct steady-state in phases B and C, with the stationary phase C yielding a higher steady-state charging energy.

The emergence of the different dynamical phases can be seen from the properties of the eigenvalues λ_{II} of the Liouvillian superoperator \mathcal{L} [58]. The quantum master equation (5) can be written compactly as $\dot{\rho} = \mathcal{L}\rho$, with the formal solution $\rho(t) = e^{\mathcal{L}t}\rho(0) = \sum_s c_s e^{\lambda_s t} \rho_s$, where λ_s denotes the s th eigenvalue of \mathcal{L} , ρ_s is the corresponding eigenmode, and the coefficient c_s is determined by the initial state. As shown in Fig. 3(b), the Liouvillian spectrum in the stationary phase (red dots) is gapless. The eigenvalue with the largest real part possesses a nonzero imaginary component, causing the QB dynamics to approach a stationary value after transient oscillations. In contrast, the spectrum in the BTC phase (blue dots) is gapped, and the leading eigenvalue has a vanishing imaginary part, giving rise to sustained coherent oscillations.

A comparison between the exact numerical results of the master equation (5) and the mean-field predictions is studied in Figs. 3(c) and 3(d). As shown in Fig. 3(c), the mean-field results converge toward the exact numerics as the atom number N increases, and the steady-state energy \mathcal{E}_{II}^{ss} approaches 0.5 with increasing Ω . However, Fig. 3(d) reveals that while \mathcal{E}_{II}^{ss} converges toward the mean-field prediction in the BTC phase, its behavior in stationary phase C appears to be different. In particular, a significant deviation from the mean-field results emerges for system sizes achievable in steady-state calculations.

To investigate whether this deviation persists in larger system size, we examine the finite time evolution of the energy in Figs. 4(a)-4(d), which allows us to access larger atom numbers N within feasible computation time. In the BTC phase, $\mathcal{E}_{II}(t)$ exhibits damped oscillations until it approaches the steady-state value 0.5 for finite atom numbers N . As N increases, $\mathcal{E}_{II}(t)$ exhibits persistent oscillations. In the stationary phases B, $\mathcal{E}_{II}(t)$ fast approaches a small steady-state value, which converges to the mean-field results with the increase of N . In the stationary phase C, we observe that for small system size, $\mathcal{E}_{II}(t)$ has a larger deviation from the mean-field results as time increases. Nevertheless, this does not invalidate the mean-field method, which is exact only in the thermodynamic limit, despite the fact that all experimental systems are inherently finite [86]. For a comparison, we show $\mathcal{E}_{II}(t)$ in the stationary phase C for larger N in Fig. 4(d) over a shorter time window. This shows how the exact numerics indeed approach the mean-field prediction for finite- N simulations. Owing to the existence of the MFB control, the stored energy in the QB array is close to full charge in the case of $\Omega/\Gamma \ll 1$, marked by the shade area in Fig. 4(d). Figure 4(e) shows the maximal $\mathcal{E}_{II}^{\text{max}}$ and ergotropy $\mathcal{W}_{II}^{\text{max}}$ versus the atom numbers N in the three different phases. For a fixed value

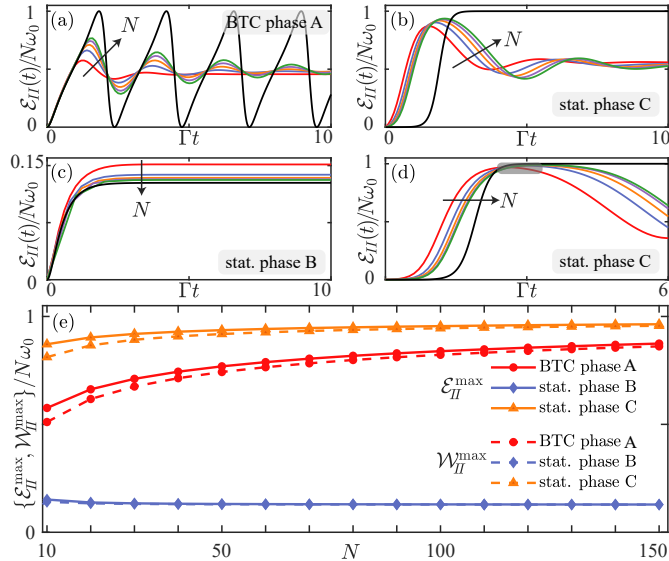


FIG. 4. (a) and (c) Stored energy $\mathcal{E}_{II}(t)$ as a function of time in the BTC phase A and stationary phase B for $\Omega/\Gamma = 1$ and $\Omega/\Gamma = 2$ with $g = 1$. (b) and (d) Stored energy $\mathcal{E}_{II}(t)$ as a function of time in the stationary phase C for $\Omega/\Gamma = 0.01$ and $g = -2$. Panels (a), (b), and (c) show $N = 10, 20, 30, 40, 50$. Panel (d) shows instead more extensive comparison for $N = 200, 600, 1000, 1400, 1800$. (e) Maximal energy \mathcal{E}_{II}^{max} and ergotropy \mathcal{W}_{II}^{max} versus N in different phases.

of N , both \mathcal{E}_{II}^{max} and \mathcal{W}_{II}^{max} are the highest in the stationary phase C. As N increases, these quantities remain nearly constant but small in the phase B. In contrast, in the stationary phase C and BTC phase, \mathcal{E}_{II}^{max} and \mathcal{W}_{II}^{max} gradually approach unity with increasing N . In all phases, \mathcal{W}_{II}^{max} converges toward \mathcal{E}_{II}^{max} as N grows.

V. CONCLUSIONS AND OUTLOOK

In conclusion, we have explored the charging performance of the driven-dissipation QB with MFB control in two different setups based on waveguide-QED systems. In the single-atom-QB scenario, the steady-state energy and ergotropy of the QB can be remarkably enhanced by the MFB control. Extending to the multiple-atom case, we showed that the MFB control and the laser driving cause the steady-state energy charging to exhibit three different dynamical phases. These rich dynamical phases provide us a valid method to control the charging performance of the QB on demand. Our results advance the realization of QBs and provide a guideline for manipulating the charging process in open quantum systems. Future work could investigate physically richer settings for QB charging in the driven-dissipative regime, such as exploring the role of time delays between coupling points of emitters [87–90], using the rich interference effects in giant atoms [91], and extending the scheme to multi-level atoms [92, 93].

ACKNOWLEDGMENTS

We thank F. Carollo, X.-Z. Ge, and Y.-H. Zhou for helpful discussions. We also acknowledge the use of the open source Python numerical packages QuTiP [94, 95]. This work is partially financially supported by Innovation Program for Quantum Science and Technology 2023ZD0300600, Guangdong Provincial Quantum Science Strategic Initiative (No. GDZX2200001), Hong Kong Research Grant Council (RGC) under Grant No. 15213924, National Natural Science Foundation of China under Grants No. 62173288.

[1] J. M. R. Parrondo, J. M. Horowitz, and T. Sagawa, Thermodynamics of information, *Nat. Phys.* **11**, 131 (2015).
[2] J. Millen and A. Xuereb, Perspective on quantum thermodynamics, *New J. Phys.* **18**, 011002 (2016).
[3] A. Auffèves, Quantum technologies need a quantum energy initiative, *PRX Quantum* **3**, 020101 (2022).
[4] R. Alicki and M. Fannes, Entanglement boost for extractable work from ensembles of quantum batteries, *Phys. Rev. E* **87**, 042123 (2013).

- [5] F. Campaioli, F. A. Pollock, F. C. Binder, L. Céleri, J. Goold, S. Vinjanampathy, and K. Modi, Enhancing the Charging Power of Quantum Batteries, *Phys. Rev. Lett.* **118**, 150601 (2017).
- [6] G. M. Andolina, M. Keck, A. Mari, M. Campisi, V. Giovannetti, and M. Polini, Extractable Work, the Role of Correlations, and Asymptotic Freedom in Quantum Batteries, *Phys. Rev. Lett.* **122**, 047702 (2019).
- [7] S. Ghosh, T. Chanda, and A. Sen(De), Enhancement in the performance of a quantum battery by ordered and disordered interactions, *Phys. Rev. A* **101**, 032115 (2020).
- [8] F. H. Kamin, F. T. Tabesh, S. Salimi, and A. C. Santos, Entanglement, coherence, and charging process of quantum batteries, *Phys. Rev. E* **102**, 052109 (2020).
- [9] A. Crescente, M. Carrega, M. Sassetto, and D. Ferraro, Ultrafast charging in a two-photon Dicke quantum battery, *Phys. Rev. B* **102**, 245407 (2020).
- [10] S. Seah, M. Perarnau-Llobet, G. Haack, N. Brunner, and S. Nimmrichter, Quantum Speed-Up in Collisional Battery Charging, *Phys. Rev. Lett.* **127**, 100601 (2021).
- [11] Y. Huangfu and J. Jing, High-capacity and high-power collective charging with spin chargers, *Phys. Rev. E* **104**, 024129 (2021).
- [12] J.-Y. Gyhm, D. Šafránek, and D. Rosa, Quantum Charging Advantage Cannot Be Extensive without Global Operations, *Phys. Rev. Lett.* **128**, 140501 (2022).
- [13] H.-L. Shi, S. Ding, Q.-K. Wan, X.-H. Wang, and W.-L. Yang, Entanglement, Coherence, and Extractable Work in Quantum Batteries, *Phys. Rev. Lett.* **129**, 130602 (2022).
- [14] G. Zhu, Y. Chen, Y. Hasegawa, and P. Xue, Charging Quantum Batteries via Indefinite Causal Order: Theory and Experiment, *Phys. Rev. Lett.* **131**, 240401 (2023).
- [15] A. C. Santos, B. Çakmak, S. Campbell, and N. T. Zinner, Stable adiabatic quantum batteries, *Phys. Rev. E* **100**, 032107 (2019).
- [16] F.-Q. Dou, Y.-J. Wang, and J.-A. Sun, Closed-loop three-level charged quantum battery, *Europhys. Lett.* **131**, 43001 (2020).
- [17] S.-F. Qi and J. Jing, Magnon-mediated quantum battery under systematic errors, *Phys. Rev. A* **104**, 032606 (2021).
- [18] D. Rossini, G. M. Andolina, D. Rosa, M. Carrega, and M. Polini, Quantum Advantage in the Charging Process of Sachdev-Ye-Kitaev Batteries, *Phys. Rev. Lett.* **125**, 236402 (2020).
- [19] J. Kim, J. Murugan, J. Olle, and D. Rosa, Operator delocalization in quantum networks, *Phys. Rev. A* **105**, L010201 (2022).
- [20] L. Fusco, M. Paternostro, and G. De Chiara, Work extraction and energy storage in the Dicke model, *Phys. Rev. E* **94**, 052122 (2016).
- [21] D. Ferraro, M. Campisi, G. M. Andolina, V. Pellegrini, and M. Polini, High-Power Collective Charging of a Solid-State Quantum Battery, *Phys. Rev. Lett.* **120**, 117702 (2018).
- [22] A. Crescente, M. Carrega, M. Sassetto, and D. Ferraro, Ultrafast charging in a two-photon dicke quantum battery, *Phys. Rev. B* **102**, 245407 (2020).
- [23] D.-L. Yang, F.-M. Yang, and F.-Q. Dou, Three-level Dicke quantum battery, *Phys. Rev. B* **109**, 235432 (2024).
- [24] W. Lu, J. Chen, L.-M. Kuang, and X. Wang, Optimal state for a tavis-cummings quantum battery via the bethe ansatz method, *Phys. Rev. A* **104**, 043706 (2021).
- [25] J.-X. Liu, H.-L. Shi, Y.-H. Shi, X.-H. Wang, and W.-L. Yang, Entanglement and work extraction in the central-spin quantum battery, *Phys. Rev. B* **104**, 245418 (2021).
- [26] L. Peng, W.-B. He, S. Chesi, H.-Q. Lin, and X.-W. Guan, Lower and upper bounds of quantum battery power in multiple central spin systems, *Phys. Rev. A* **103**, 052220 (2021).
- [27] D. Farina, G. M. Andolina, A. Mari, M. Polini, and V. Giovannetti, Charger-mediated energy transfer for quantum batteries: An open-system approach, *Phys. Rev. B* **99**, 035421 (2019).
- [28] F. Barra, Dissipative Charging of a Quantum Battery, *Phys. Rev. Lett.* **122**, 210601 (2019).
- [29] F. Pirmoradian and K. Mølmer, Aging of a quantum battery, *Phys. Rev. A* **100**, 043833 (2019).
- [30] W. Chang, T. R. Yang, H. Dong, L. Fu, X. Wang, and Y.-Y. Zhang, Optimal building block of multipartite quantum battery in the driven-dissipative charging, *New J. Phys.* **23**, 103026 (2021).
- [31] W. S. Martins, F. Carollo, W. Li, K. Brandner, and I. Lesanovsky, Rydberg-ion flywheel for quantum work storage, *Phys. Rev. A* **108**, L050201 (2023).
- [32] R. R. Rodríguez, B. Ahmadi, P. Mazurek, S. Barzanjeh, R. Alicki, and P. Horodecki, Catalysis in charging quantum batteries, *Phys. Rev. A* **107**, 042419 (2023).
- [33] B. Ahmadi, P. Mazurek, P. Horodecki, and S. Barzanjeh, Nonreciprocal Quantum Batteries, *Phys. Rev. Lett.* **132**, 210402 (2024).
- [34] A. Catalano, S. Giampaolo, O. Morsch, V. Giovannetti, and F. Franchini, Frustrating Quantum Batteries, *PRX Quantum* **5**, 030319 (2024).
- [35] S. Pokhrel and J. Gea-Banacloche, Large collective power enhancement in dissipative charging of a quantum battery, *Phys. Rev. Lett.* **134**, 130401 (2025).
- [36] F. Kamin, F. Tabesh, S. Salimi, F. Kheirandish, and A. C. Santos, Non-Markovian effects on charging and self-discharging process of quantum batteries, *New J. Phys.* **22**, 083007 (2020).
- [37] F. T. Tabesh, F. H. Kamin, and S. Salimi, Environment mediated charging process of quantum batteries, *Phys. Rev. A* **102**, 052223 (2020).

[38] M.-L. Song, L.-J. Li, X.-K. Song, L. Ye, and D. Wang, Environment-mediated entropic uncertainty in charging quantum batteries, *Phys. Rev. E* **106**, 054107 (2022).

[39] W.-L. Song, H.-B. Liu, B. Zhou, W.-L. Yang, and J.-H. An, Remote Charging and Degradation Suppression for the Quantum Battery, *Phys. Rev. Lett.* **132**, 090401 (2024).

[40] Z.-G. Lu, G. Tian, X.-Y. Lü, and C. Shang, Topological Quantum Batteries, *Phys. Rev. Lett.* **134**, 180401 (2025).

[41] S.-Y. Bai and J.-H. An, Floquet engineering to reactivate a dissipative quantum battery, *Phys. Rev. A* **102**, 060201(R) (2020).

[42] J. Q. Quach and W. J. Munro, Using Dark States to Charge and Stabilize Open Quantum Batteries, *Phys. Rev. Appl.* **14**, 024092 (2020).

[43] Y. Yao and X. Q. Shao, Stable charging of a Rydberg quantum battery in an open system, *Phys. Rev. E* **104**, 044116 (2021).

[44] M. T. Mitchison, J. Goold, and J. Prior, Charging a quantum battery with linear feedback control, *Quantum* **5**, 500 (2021).

[45] Y. Yao and X. Q. Shao, Optimal charging of open spin-chain quantum batteries via homodyne-based feedback control, *Phys. Rev. E* **106**, 014138 (2022).

[46] W.-L. Song, J.-L. Wang, B. Zhou, W.-L. Yang, and J.-H. An, Self-Discharging Mitigated Quantum Battery, *Phys. Rev. Lett.* **135**, 020405 (2025).

[47] Y. Yao and X. Q. Shao, Reservoir-assisted quantum battery charging at finite temperatures, *Phys. Rev. A* **111**, 062616 (2025).

[48] R.-H. Zheng, W. Ning, Z.-B. Yang, Y. Xia, and S.-B. Zheng, Demonstration of dynamical control of three-level open systems with a superconducting qutrit, *New J. Phys.* **24**, 063031 (2022).

[49] C.-K. Hu, J. Qiu, P. J. P. Souza, J. Yuan, Y. Zhou, L. Zhang, J. Chu, X. Pan, L. Hu, J. Li, Y. Xu, Y. Zhong, S. Liu, F. Yan, D. Tan, R. Bachelard, C. J. Villas-Boas, A. C. Santos, and D. Yu, Optimal charging of a superconducting quantum battery, *Quantum Sci. Technol.* **7**, 045018 (2022).

[50] I. M. de Buy Wenniger, S. E. Thomas, M. Maffei, S. C. Wein, M. Pont, N. Belabas, S. Prasad, A. Harouri, A. Lemaître, I. Sagnes, N. Somaschi, A. Auffèves, and P. Senellart, Experimental Analysis of Energy Transfers between a Quantum Emitter and Light Fields, *Phys. Rev. Lett.* **131**, 260401 (2023).

[51] J. Q. Quach, K. E. McGhee, L. Ganzer, D. M. Rouse, B. W. Lovett, E. M. Gauger, J. Keeling, G. Cerullo, D. G. Lidzey, and T. Virgili, Superabsorption in an organic microcavity: Toward a quantum battery, *Sci. Adv.* **8**, 3160 (2022).

[52] J. Joshi and T. S. Mahesh, Experimental investigation of a quantum battery using star-topology NMR spin systems, *Phys. Rev. A* **106**, 042601 (2022).

[53] Z. Liao, X. Zeng, H. Nha, and M. S. Zubairy, Photon transport in a one-dimensional nanophotonic waveguide QED system, *Phys. Scr.* **91**, 063004 (2016).

[54] D. Roy, C. M. Wilson, and O. Firstenberg, Colloquium: Strongly interacting photons in one-dimensional continuum, *Rev. Mod. Phys.* **89**, 021001 (2017).

[55] X. Gu, A. F. Kockum, A. Miranowicz, Y.-x. Liu, and F. Nori, Microwave photonics with superconducting quantum circuits, *Phys. Rep.* **718**, 1 (2017).

[56] A. S. Sheremet, M. I. Petrov, I. V. Iorsh, A. V. Poshakinskiy, and A. N. Poddubny, Waveguide quantum electrodynamics: collective radiance and photon-photon correlations, *Rev. Mod. Phys.* **95**, 015002 (2023).

[57] S. Tirone, G. M. Andolina, G. Calajò, V. Giovannetti, and D. Rossini, Many-body enhancement of energy storage in a waveguide-QED quantum battery, *Phys. Rev. A* **112**, 013717 (2025).

[58] F. Iemini, A. Russomanno, J. Keeling, M. Schirò, M. Dalmonte, and R. Fazio, Boundary Time Crystals, *Phys. Rev. Lett.* **121**, 035301 (2018).

[59] F. Carollo, K. Brandner, and I. Lesanovsky, Nonequilibrium Many-Body Quantum Engine Driven by Time-Translation Symmetry Breaking, *Phys. Rev. Lett.* **125**, 240602 (2020).

[60] L. F. d. Prazeres, L. d. S. Souza, and F. Iemini, Boundary time crystals in collective d -level systems, *Phys. Rev. B* **103**, 184308 (2021).

[61] H. M. Wiseman, Quantum theory of continuous feedback, *Phys. Rev. A* **49**, 2133 (1994).

[62] H. M. Wiseman and G. J. Milburn, *Quantum Measurement and Control* (Cambridge University, 2009).

[63] T. Tufarelli, F. Ciccarello, and M. S. Kim, Dynamics of spontaneous emission in a single-end photonic waveguide, *Phys. Rev. A* **87**, 013820 (2013).

[64] I.-C. Hoi, A. F. Kockum, L. Tornberg, A. Pourkabirian, G. Johansson, P. Delsing, and C. M. Wilson, Probing the Quantum Vacuum with an Artificial Atom in Front of a Mirror, *Nat. Phys.* **11**, 1045 (2015).

[65] G. Calajò, Y.-L. L. Fang, H. U. Baranger, and F. Ciccarello, Exciting a Bound State in the Continuum through Multiphoton Scattering Plus Delayed Quantum Feedback, *Phys. Rev. Lett.* **122**, 073601 (2019).

[66] G. Buonaiuto, F. Carollo, B. Olmos, and I. Lesanovsky, Dynamical Phases and Quantum Correlations in an Emitter-Waveguide System With Feedback, *Phys. Rev. Lett.* **127**, 133601 (2021).

[67] J. Gough and M. R. James, Quantum Feedback Networks: Hamiltonian Formulation, *Commun. Math. Phys.* **287**, 1109 (2009).

[68] J. Gough and M. R. James, The Series Product and Its Application to Quantum Feedforward and Feedback Networks, *IEEE Trans. Autom. Control* **54**, 2530 (2009).

[69] G. Zhang and M. R. James, Quantum feedback networks and control: A brief survey, *Chin. Sci. Bull.* **57**, 2200 (2012).

[70] J. Combes, J. Kerckhoff, and M. Sarovar, The SLH framework for modeling quantum input-output networks, *Advances in Physics: X* **2**, 784 (2017).

[71] See the Supplemental Information for details on the derivation of the quantum master equation and additional supporting simulations.

[72] P. O. Guimond, B. Vermersch, M. L. Juan, A. Sharafiev, G. Kirchmair, and P. Zoller, A unidirectional on-chip photonic interface for superconducting circuits, *npj Quantum Inf.* **6**, 32 (2020).

[73] B. Kannan, A. Almanakly, Y. Sung, A. Di Paolo, D. A. Rower, J. Braumüller, A. Melville, B. M. Niedzielski, A. Karamlou, K. Serniak, A. Vepsäläinen, M. E. Schwartz, J. L. Yoder, R. Winik, J. I. Wang, T. P. Orlando, S. Gustavsson, J. A. Grover, and W. D. Oliver, On-demand directional microwave photon emission using waveguide quantum electrodynamics, *Nat. Phys.* **19**, 394 (2023).

[74] Parth S. Shah, Frank Yang, Chaitali Joshi, and Mohammad Mirhosseini, Stabilizing remote entanglement via waveguide dissipation, *PRX Quantum* **5**, 030346 (2024).

[75] A. E. Allahverdyan, R. Balian, and T. M. Nieuwenhuizen, Maximal work extraction from finite quantum systems, *Euro-physics Letters* **67**, 565 (2004).

[76] G. Francica, F. C. Binder, G. Guarnieri, M. T. Mitchison, J. Goold, and F. Plastina, Quantum coherence and ergotropy, *Phys. Rev. Lett.* **125**, 180603 (2020).

[77] C. W. Gardiner, Inhibition of Atomic Phase Decays by Squeezed Light: A Direct Effect of Squeezing, *Phys. Rev. Lett.* **56**, 1917 (1986).

[78] H. J. Carmichael, A. S. Lane, and D. F. Walls, Resonance Fluorescence from an Atom in a Squeezed Vacuum, *Phys. Rev. Lett.* **58**, 2539 (1987).

[79] D. M. Toyli, A. W. Eddins, S. Boutin, S. Puri, D. Hover, V. Bolkhovsky, W. D. Oliver, A. Blais, and I. Siddiqi, Resonance Fluorescence from an Artificial Atom in Squeezed Vacuum, *Phys. Rev. X* **6**, 031004 (2016).

[80] X.-L. Yin, H.-w. J. Lee, and G. Zhang, Giant-atom dephasing dynamics and entanglement generation in a squeezed vacuum reservoir, *Phys. Rev. A* **111**, 033707 (2025).

[81] D. A. Ivanov, T. Yu. Ivanova, S. F. Caballero-Benitez, and I. B. Mekhov, Feedback-Induced Quantum Phase Transitions using Weak Measurements, *Phys. Rev. Lett.* **124**, 010603 (2020).

[82] G. S. Agarwal and R. R. Puri, Cooperative behavior of atoms irradiated by broadband squeezed light, *Phys. Rev. A* **41**, 3782 (1990).

[83] W. Song, W. Yang, J. An, and M. Feng, Dissipation-assisted spin squeezing of nitrogen-vacancy centers coupled to a rectangular hollow metallic waveguide, *Opt. Express* **25**, 19226 (2017).

[84] S.-Y. Bai and J.-H. An, Generating Stable Spin Squeezing by Squeezed-Reservoir Engineering, *Phys. Rev. Lett.* **127**, 083602 (2021).

[85] R. Mattes, I. Lesanovsky, and F. Carollo, Entangled timecrystal phase in an open quantum light-matter system, *Phys. Rev. A* **108**, 062216 (2023).

[86] F. Carollo and I. Lesanovsky, Applicability of Mean-Field Theory for Time-Dependent Open Quantum Systems with Infinite-Range Interactions, *Phys. Rev. Lett.* **133**, 150401 (2024).

[87] H. Pichler and P. Zoller, Photonic Circuits with Time Delays and Quantum Feedback, *Phys. Rev. Lett.* **116**, 093601 (2016).

[88] K. Vodenkova and H. Pichler, Continuous Coherent Quantum Feedback with Time Delays: Tensor Network Solution, *Phys. Rev. X* **14**, 031043 (2024).

[89] B. Windt, M. Bello, D. Malz, and J. I. Cirac, Effects of Retardation on Many-Body Superradiance in Chiral Waveguide QED, *Phys. Rev. Lett.* **134**, 173601 (2025).

[90] C. Barahona-Pascual, H. Jiang, A. C. Santos, J. José García-Ripoll, Time-delayed collective dynamics in waveguide QED and bosonic quantum networks, *arXiv: 2505.02642*.

[91] A. F. Kockum, Quantum optics with giant atoms—the first five years, *Mathematics for Industry* (Springer Singapore, Singapore, 2021), pp. 125–146.

[92] O. A. Iversen and T. Pohl, Strongly Correlated States of Light and Repulsive Photons in Chiral Chains of Three-Level Quantum Emitters, *Phys. Rev. Lett.* **126**, 083605 (2021).

[93] A. N. Poddubny, S. Rosenblum, and B. Dayan, How Single-Photon Switching Is Quenched with Multiple Λ -level atoms, *Phys. Rev. Lett.* **133**, 113601 (2024).

[94] J. Johansson, P. Nation, and F. Nori, Qutip: An open-source python framework for the dynamics of open quantum systems, *Comput. Phys. Commun.* **183**, 1760 (2012).

[95] J. Johansson, P. Nation, and F. Nori, Qutip 2: A python framework for the dynamics of open quantum systems, *Comput. Phys. Commun.* **184**, 1234 (2013).